International Journal of Thermal Sciences 77 (2014) 158–164

Contents lists available at ScienceDirect

International Journal of Thermal Sciences

journal homepage: www.elsevier.com/locate/ijts

Performance characteristics of a low concentrated photovoltaic–thermoelectric hybrid power generation device

Tianjun Liao, Bihong Lin*, Zhimin Yang

College of Information Science and Engineering, Huaqiao University, Xiamen, Fujian 361021, China

ARTICLE INFO

Article history:
Received 21 May 2013
Received in revised form
20 October 2013
Accepted 22 October 2013
Available online 6 December 2013

Keywords:
Low concentrated photovoltaic cells
Thermoelectric generator
Performance characteristics
Non-equilibrium thermodynamics

ABSTRACT

A theoretical model of a hybrid power generation device consisting of a low concentrated photovoltaic (CPV) module and a thermoelectric generator (TEG) is established in this paper. The expressions for the efficiency and power output of the hybrid device are derived and the performance characteristics of the device are presented and discussed in detail, based on non-equilibrium thermodynamics theory and law of conservation of energy. The maximum power output of the hybrid device is calculated numerically and the load electric resistances of the CPV and TEG are determined optimally. The influences of several important factors such as the thermal conductance between the CPV and the TEG, the current of the CPV, the solar irradiation, the concentrating ratio and the figure of merit of the TEG on the power output of the hybrid device are analyzed. It is found that there exist certain optimum criteria for some important parameters. The results obtained here may provide some useful criteria for the optimal design and performance improvements of a typical irreversible CPV–TEG hybrid device and other similar hybrid system as well.

1. Introduction

Energy is the foundation of national economic development and the construction of modern civilization. Due to growing concerns about global fossil energy, environment and climate, the research and development of renewable clean energies has received more and more attention. Solar energy is one of the most important clean energy and solar photovoltaic (PV) module is currently one of the most important components in solar energy applications. The PV industry of silicon solar cells has obtained rapid development in recent years. However, the high cost of high purity silicon materials and its tedious manufacture process and the limited efficiency of solar energy conversion have hindered its massive applications [1]. Using optical concentrators such as parabolic dishes and lenses to concentrate sunlight on PV cells in order to increase the intensity of incident irradiation is one method used to acquire more power per unit of area of PV cells [2]. Nevertheless, only a small fraction of the incident to the PV cell sunshine is converted into electrical energy. In the cell, most of the incident energy of the sun will be converted into thermal energy and may cause the junction temperature rise unless the heat is effective dissipated to the environment [3]. What's more, CPV systems may suffer from a drop in efficiency with the rise in temperature due to increased resistance [2,3]. Photovoltaic/thermal (PV/T) is the most common active cooling method and can simultaneously provide electricity and heat [4–8]. Therefore, it can achieve higher conversion efficiency of the absorbed solar radiation than that of the standard PV module. When properly designed, PV/T systems can extract heat from PV modules, heating water or air to reduce the operating temperature of the PV modules and keep the electrical efficiency at a sufficient level [9]. In addition, it has been proposed to use the thermal waste by attaching thermoelectric generators (TEG) to the back of PV modules, to form a CPV–TEG hybrid device [10]. Due to the temperature difference between the back side of the PV module and the environment, the additional electricity can be generated by the TEG and the efficiency of the hybrid device may be improved.

The theory and technology of PV–TEG have been discussed and developed extensively during the past years [10–27]. Van Sark [10] and Wang et al. [21] proposed to use the thermal waste by attaching the TEG to the back of PV modules for energy harvesting and investigated theoretically and experimentally the performance of the hybrid devices. Vorobiev et al. [7], Kraemer et al. [17] and Xing Ju et al. [22] mentioned and developed a spectrum splitting PV–TEG hybrid system and shown that this hybrid system could help maximize the conversion efficiency. Zhang and Chau [19,20] designed and implemented PV–TEG hybrid systems for hybrid

* Corresponding author. Tel.: +86 059 261 623 88.
E-mail address: bhlin@hqu.edu.cn (B. Lin).

1290-0729/$ – see front matter © 2013 Elsevier Masson SAS. All rights reserved.
http://dx.doi.org/10.1016/j.ijthermalsci.2013.10.013

electric vehicles based on TEG can collect waste heat of internal combustion engines and solar cells for converting solar energy. The results provide useful information for developing energy policies and estimating their environment impacts.

However, so far, there have been few theoretical performance analysis and optimization for the CPV–TEG hybrid device. Thus, in the present paper, we will construct a new irreversible hybrid device composed of a low concentrating photovoltaic module and a semiconductor thermoelectric generator which can conveniently utilize the waste heat produced in a CPV module. Based on the current models of the PV module and thermoelectric generator, some expressions for some key parameters in the hybrid device are derived. The performance characteristics of the hybrid system are revealed. The effects of the thermal conductance between the CPV and the TEG, the concentrating ratio, and the dimensionless figure of merit of the TEG on the performance of the hybrid device are analyzed in detail. The optimum criteria of some main performance parameters are determined. Some significant results are obtained.

2. A theoretical model of an irreversible CPV–TEG hybrid device

The hybrid device considered here is consisted of a concentrator, a PV module, and a TEG module, as shown in Fig. 1, where R_{L1} and R_{L2} are, respectively, the load resistances of CPV module and TEG, T is the temperature of CPV, T_H and T_L are, respectively, the temperatures of the hot side and the cold side of TEG module. In this hybrid device, the CPV module acts as the high-temperature heat reservoir of the TEG module for a further production of power. By using such a hybrid device, the heat produced in the CPV can be availably utilized, and thus, the performance of the system can be improved further. In the following, we will analyze the performance of two composing parts, the CPV module, and TEG module, respectively, and then synthetically investigate the performance characteristics of the hybrid device.

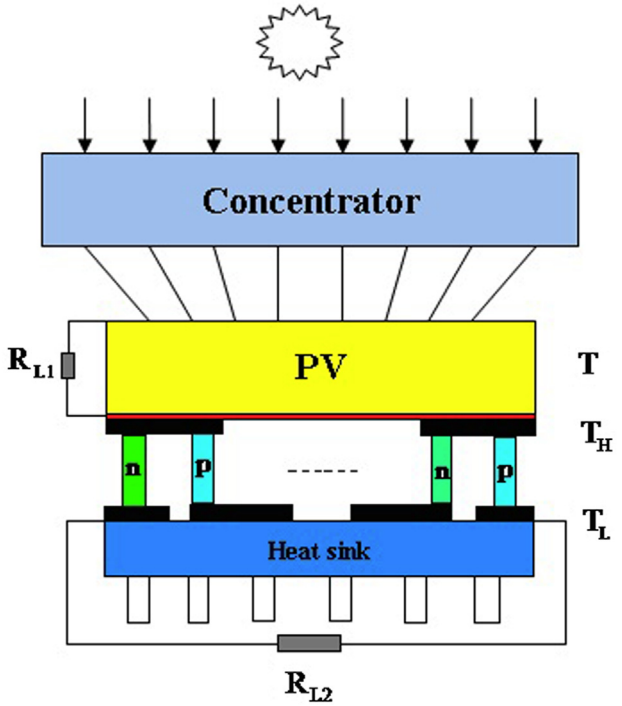

Fig. 1. A schematic diagram of the CPV–TEG hybrid device.

2.1. The power output and efficiency of CPV module

The CPV module consists of a concentrator to concentrate the sunlight and a PV module, as shown in Fig. 1. The concentrated sunlight is focused on the PV module. The energy balance for the absorptive surface of the PV module yields [23,25],

$$CG\eta_0 A_{PV} = \dot{Q}_{in} + \varepsilon\sigma A_{PV}\left(T^4 - T_0^4\right) + hA_{PV}(T - T_0) \tag{1}$$

where $\dot{Q}_{in}$ is the energy transferred to the PV module per unit time, C is the optical concentration ratio, G is the solar irradiation, η_0 is the optical efficiency of the concentrator, A_{PV} is the area of PV module, ε is the emittance of the selective surface facing the incoming solar radiation, h is the heat transfer coefficient of the PV surface, σ is the Stefan–Boltzmann constant, T is the temperature of the PV module, and T_0 is the ambient temperature.

It is assumed that a PV module can be represented by an irradiance-dependent current source in parallel with a diode [18]. The equivalent circuit of a PV module is shown in Fig. 2. The I–V characteristic is determined by the following equation [18,28]:

$$I = n_p I_L - n_p I_o = n_p I_L - n_p I_S\left\{\exp\left[\frac{q(V + IR_S)}{AK_b T n_s}\right] - 1\right\} \tag{2}$$

where I, I_L, I_0 and I_S are, respectively, the PV array output current, the photocurrent, the diode reverse current and the diode reverse saturation current, q is the charge of an electron, R_S is the intrinsic series resistance of the PV cell, K_b is the Boltzmann constant, n_p and n_s are, respectively, the number of cells in parallel and in series, and A is the diode ideality factor [29,30], which can all be dependent on bias voltage and temperature. It is an indicator of the behavioral proximity of the device under test, to an ideal diode. For an ideal diode, A is however constant and usually, has a value between 1 and 2 [31].

In general, the photocurrent I_L depends on the solar radiation and the cell temperature. It can be expressed as [18,22,28],

$$I_L = \frac{G}{G_r}\left[CI_{SCR} + K_I(T - T_r)\right] \tag{3}$$

where T_r and G_r are, respectively, the PV cell reference temperature and solar irradiation, I_{SCR} is the cell short-circuit current at reference temperature and radiation, and K_I is the short-circuit current temperature coefficient. In addition, the PV cell reverse saturation current I_S varies with temperature and is given by Refs. [18,22,28],

$$I_S = CI_r\left(\frac{T}{T_r}\right)^3 \exp\left[\frac{E_g q}{K_b}\left(\frac{1}{T_r} - \frac{1}{T}\right)\right] \tag{4}$$

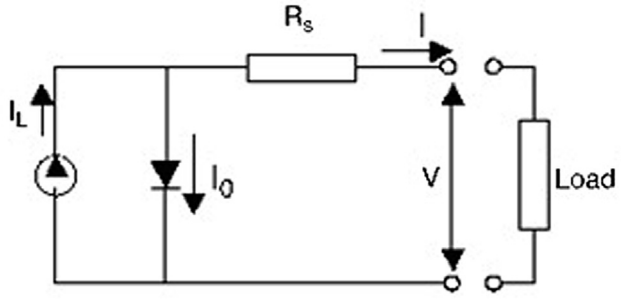

Fig. 2. Equivalent circuit of a PV cells.

where E_g and I_r are the band-gap energy of the semiconductor materials used in the PV cell and the reverse saturation current at T_r, respectively.

According to the equation above and Fig. 2, the power output and the efficiency of CPV module are, respectively, given by

$$P_{PV} = I^2 R_{L1} \tag{5}$$

and

$$\eta_{PV} = \frac{P_{PV}}{CGA_{PV}\eta_0} = \frac{I^2 R_{L1}}{CGA_{PV}\eta_0} \tag{6}$$

In the present article, the Siemens SP75 PV cell using the polycrystalline technology is chosen as the PV module in Fig. 1 and its main parameters are shown in Table 1.

2.2. The power output of a multi-couple TEG

Heat can be used to generate electricity based on the Peltier and Seebeck effects of thermoelectric materials. A TEG which converts part of an amount of heat absorbed directly into electrical power is just one of the power sources of unconventional nature which are being pursued vigorously in research and development. The basic unit of a TEG is composed of an n-type semiconductor element and a p-type semiconductor element. The lower part of Fig. 1 shows a schematic diagram of a multi-couple TEG module, which involves a large number of semiconductor elements connected electrically in series by metal strips and thermally in parallel. It is assumed that $\dot{Q}_H$ and $\dot{Q}_L$ are, respectively, the net rate of heat input from the source to the thermoelectric device and the net rate of heat rejection from the thermoelectric device to the heat sink and the current within the TEG module is to flow in one dimension. From Fig. 1, one obtains the heat balance equations as [26,32–35]

$$\dot{Q}_H = \alpha I_{TE} T_H - \frac{1}{2} I_{TE}^2 R + K(T_H - T_L) \tag{7}$$

and

$$\dot{Q}_L = \alpha I_{TE} T_L + \frac{1}{2} I_{TE}^2 R + K(T_H - T_L) \tag{8}$$

where $\alpha = N(\alpha_p - \alpha_n)$, $R = N(\rho_p l_p/S_p + \rho_n l_n/S_n)$ and $K = N(k_p S_p/l_p + k_n S_n/l_n)$ are, respectively, the total Seebeck coefficient, electrical resistance and thermal conductance of a multi-couple TEG, k is the thermal conductivity, ρ is the electrical resistivity, N is the total number of couples, I_{TE} is the working electrical current, l and S are the length and cross-sectional area of a semiconductor element, and the subscripts n and p designate the n- and p-type elements, respectively. To be sure, n-type and p-type materials don"t have the same transport properties. In this paper, eleven commercial CP2-127-06 Melcor thermoelectric modules are chosen as the TEG module in Fig. 1 and its main parameters are shown in Table 2 [36,37]. In general, α, k and ρ of a semiconductor element are changing with the operating temperature. They can be calculated using equations below as [36,37]

$$\alpha_p - \alpha_n = \left(44448.0 + 1861.2T_m - 1.981T_m^2\right) \times 10^{-9} \tag{9}$$

$$k_p + k_n = \left(125210 - 555.4T_m + 0.8262T_m^2\right) \times 10^{-4} \tag{10}$$

and

$$\rho_p + \rho_n = \left(10224.0 + 326.8T_m + 1.2558T_m^2\right) \times 10^{-10} \tag{11}$$

respectively, where $T_m = (T_H + T_L)/2$ is the average temperature of a TEG module.

Using Eqs. (7) and (8), the power output of a multi-couple TEG can be given by Refs. [26,32–35]

$$P_{TE} = \dot{Q}_H - \dot{Q}_L = I_{TE}[\alpha(T_H - T_L) - I_{TE}R] = I_{TE}^2 R_{L2}. \tag{12}$$

Appling Eq. above, I_{TE} can be expressed as

$$I_{TE} = \frac{\alpha(T_H - T_L)}{R + R_{L2}}. \tag{13}$$

Thus, the power output of a multi-couple TEG can be rewritten as

$$P_{TE} = KT_L\left[\left(\frac{T_H}{T_L} - 1\right)j - \frac{j^2}{ZT_L}\right], \tag{14}$$

where $Z = \alpha^2/(KR)$ and $j = I_{TE}\alpha/K$ are the figure of merit and the dimensionless current of the TEG, respectively. It is seen clearly from Eq. (14) that only when $0 < j < Z(T_H - T_L)$, can the TEG in the hybrid device begin to work as a generator with the power out $P_{TE} > 0$.

2.3. The power output and efficiency of hybrid device

Assuming the heat transfer between the CPV and the hot side of the TEG module obeys Newton's law [26], one can obtain the rate of heat exchange from the CPV to the TEG as

$$\dot{Q}_H = U_h A_h (T - T_H) \tag{15}$$

where U_h and A_h are the overall heat-transfer coefficients of the heat exchangers at the hot side and heat-transfer area of the hot junctions of a multi-couple TEG, respectively.

There are two forms of the waste heat from the CPV. One part is transferred to the hot junction of the TEG from the CPV and the

Table 1
Parameters of Siemens SP75 photovoltaic cells.

Parameter	Symbol	Value
Maximum output power	P_{max}	75 W
Short-circuit current	I_{SCR}	4.8 A
Open circuit voltage	V_{oc}	21.7 V
Diode ideality factor	A	1.5
Short-circuit current temperature coefficient	K_I	2.06 mA K^{-1}
Reverse saturation current at reference temperature	I_{or}	0.118 μA
Area of PV module	A_{PV}	0.6324 m^2
Number of strings in parallel	n_p	1
Number of cells in series	n_s	36
Band-gap energy of the semiconductor	E_g	1.12 eV
Reference temperature	T_r	300 K
Reference solar irradiation	G_r	1000 W m^{-2}

Table 2
Parameters of CP2-127-06 Melcor thermoelectric module [35,36].

Seebeck coefficient of a TE couple	$\alpha_p - \alpha_n$	$(44448.0 + 1861.2T_m - 1.981T_m^2) \times 10^{-9}$ V K^{-1}
Electrical resistivity of a TE couple	$\rho_p + \rho_n$	$(10224.0 + 326.8T_m + 1.2558T_m^2) \times 10^{-10}$ Ωm
Thermal conductivity of a TE couple	$k_p + k_n$	$(125{,}210 - 555.4T_m + 0.8262T_m^2) \times 10^{-4}$ W m^{-1} K^{-1}
Geometry characteristics	$S_p/l_p = S_n/l_n$	2.96×10^{-3} m
Total number of couples	N	127

other part called heat leak is directly released to the environment due to heat exchange between the TEG and surroundings. When heat transfer between the TEG and surrounding obeys a linear law, one has

$$\dot{Q}_{\text{loss}} = K_0(T_{\text{H}} - T_0) \tag{16}$$

where K_0 is the overall heat leak coefficient including conduction, convection and radiation. Based on the first law of thermodynamic, the heat flow rate from the CPV to the TEG may be expressed as

$$\dot{Q}_{\text{H}} = \dot{Q}_{\text{in}} - P_{\text{PV}} - \dot{Q}_{\text{loss}} \tag{17}$$

Substituting Eqs. (1), (5), (7), (13) and (16) into Eq. (17), one can obtain the energy balance for the TEG module as

$$\frac{Z(T_{\text{H}} - T_{\text{L}})^2}{2(1+R_{\text{L2}}/R)^2} - \frac{ZT_{\text{H}}(T_{\text{H}} - T_{\text{L}})}{(1+R_{\text{L2}}/R)} + \frac{A_{\text{PV}}}{K}\left[CG\eta_0 - \varepsilon\sigma\left(T^4 - T_0^4\right) - h(T - T_0)\right] - \frac{I^2R_{\text{L1}}}{K} - (T_{\text{H}} - T_{\text{L}}) - \frac{K_0}{K}(T_{\text{H}} - T_0) = 0 \tag{18}$$

Similarly, substituting Eqs. (1), (5), (15) and (16) into (17) gives

$$A_{\text{PV}}\left[CG\eta_0 - \varepsilon\sigma\left(T^4 - T_0^4\right) - h(T - T_0)\right] - I^2R_{\text{L1}} - K_0(T_{\text{H}} - T_0) - U_{\text{h}}A_{\text{h}}(T - T_{\text{H}}) = 0 \tag{19}$$

Using Eqs. (18) and (19), one can determine the temperatures T and T_{H} for different load resistances R_{L1} of CPV and load resistances R_{L2} of TEG module. By using Eqs. (5), (14), (18) and (19), the expressions of the power output and efficiency for the hybrid device may be derived as follows

$$P = P_{\text{PV}} + P_{\text{TE}} = I^2R_{\text{L1}} + KT_{\text{L}}\left[(T_{\text{H}}/T_{\text{L}} - 1)j - j^2/(ZT_{\text{L}})\right] \tag{20}$$

$$\eta = \frac{P}{CGA_{\text{PV}}\eta_0} = \frac{I^2R_{\text{L1}} + KT_{\text{L}}\left[(T_{\text{H}}/T_{\text{L}} - 1)j - j^2/(ZT_{\text{L}})\right]}{CGA_{\text{PV}}\eta_0} \tag{21}$$

Using Eqs. (18)–(20), one can analyze and optimize the performance characteristics of the hybrid device.

3. The performance characteristics and optimal performance of hybrid device

It is seen from Eqs. (20) and (21) that the performance of the hybrid device depends on a series of thermodynamic and thermoelectric parameters such as the working temperature T, current I, optical concentration ratio C, emittance ε and area A_{PV} in the CPV, the figure of merit Z, thermal conductance K and dimensionless current j in the TEG and so on. Below numerical calculations are carried out based on the parameters summarized in Tables 1 and 2. The values of these parameters kept constant unless mentioned specifically as follows: $\eta_0 = 0.95$, $\varepsilon = 0.85$, $\sigma = 5.67 \times 10^{-8}\text{W m}^{-2}\text{ K}^{-4}$, $K_0/K = 0.8$, $S_{\text{p}}/l_{\text{p}} = S_{\text{n}}/l_{\text{n}} = 2.96 \times 10^{-3}$ m, $N = 127$, $T_{\text{L}} = 300$ K and $T_0 = 300$ K.

Using Eqs. (2)–(4), (18)–(20), and data in Tables 1 and 2, one can generate the curves of the power output of the CPV and hybrid device varying with the current, as shown as Fig. 3, where $R_{\text{L2}}/R = 1$, $S_{\text{p}}/l_{\text{p}} = S_{\text{n}}/l_{\text{n}}$, $G = 800$ W m^{-2}, $C = 5$ and $ZT_{\text{L}} = 1.0$. Similarly, one can plot the curves of the dimensionless current and the working temperature varying with the current, as shown in Figs. 4 and 5, where the values of the parameters R_{L2}/R, $U_{\text{h}}A_{\text{h}}$, C, G and ZT_{L} are the same as those used in Fig. 3. It can be seen

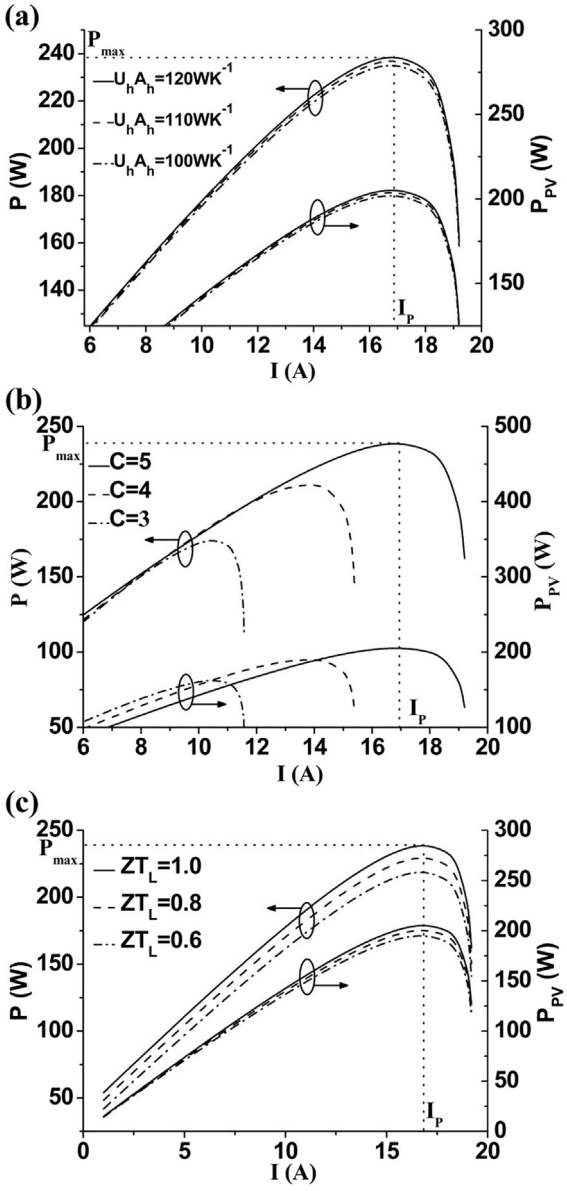

Fig. 3. The curves of the power output of the hybrid device, and CPV varying with the current for some given parameters: (a) $G = 800$ W m^{-2}, $C = 5$, $ZT_{\text{L}} = 1.0$, $R_{\text{L2}}/R = 1$, and $U_{\text{h}}A_{\text{h}} = 100$ W K^{-1}, 110 W K^{-1} and 120 W K^{-1}, (b) $G = 800$ W m^{-2}, $U_{\text{h}}A_{\text{h}} = 120$ W K^{-1}, $ZT_{\text{L}} = 1.0$, $R_{\text{L2}}/R = 1$, and $C = 3$, 4 and 5, and (c) $G = 800$ W m^{-2}, $C = 5$, $U_{\text{h}}A_{\text{h}} = 120$ W K^{-1}, $R_{\text{L2}}/R = 1$, and $ZT_{\text{L}} = 0.6$, 0.8 and 1.0.

from Fig. 3 that the power output P first increases and then decreases as the current I is increased. It clearly shows that there are local optimal values of the current I at which the power output P attains its local maximum value for a given set of operating parameters. Thus, the optimal current I_{P} is an important performance parameters of a CPV–TEG hybrid device. Fig. 3(b) shows that the larger the optical concentration ratio C is, the larger the maximum power output P_{max} and corresponding optimal current I_{P}. This implies that in order to improve the performance of the hybrid device, the optical concentration ratio should be improved. It can be seen from Fig. 4 that the dimensionless current j is not a monotonic function of the current I of the CPV and there exists a minimum j_{min} for a given current I_{P}. The dimensionless current j will increase with thermal conductance $U_{\text{h}}A_{\text{h}}$ between the CPV and the TEG, concentrating ratio C

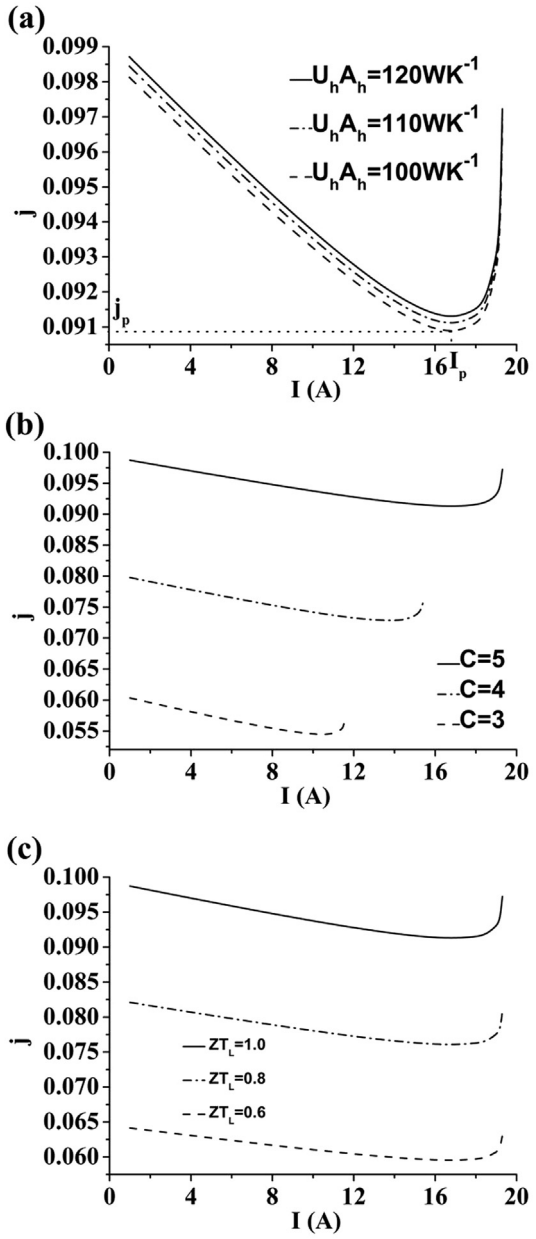

Fig. 4. The curves of the dimensionless current varying with the current, where the values of the parameters R_{L2}/R, U_hA_h, C, G and ZT_L are the same as those used in Fig. 3.

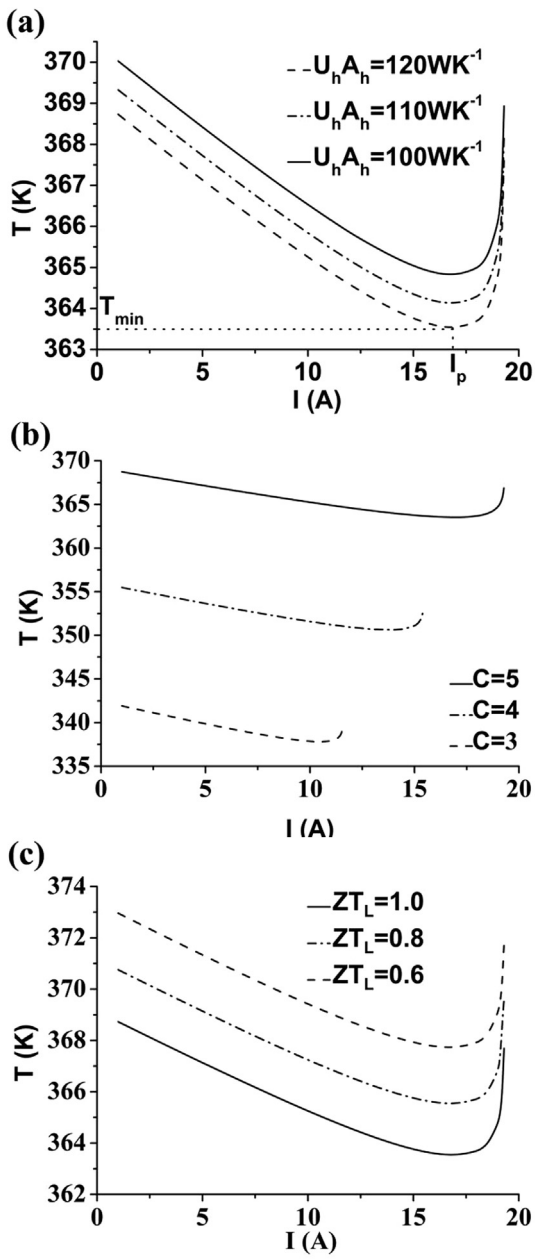

Fig. 5. The curves of the working temperature varying with the current, where the values of the parameters R_{L2}/R, U_hA_h, C, G and ZT_L are the same as those used in Fig. 3.

and figure of merit of the TEG ZT_L. Fig. 5 shows that the operating temperature T of the CPV module will decrease with increasing thermal conductance U_hA_h and figure of merit ZT_L of the TEG module and will increase with concentrating ratio C. It can also be seen from Fig. 3(a) and (c) that for some given parameters, the larger the U_hA_h and ZT_L are, the better the performance of the hybrid device. Fig. 3 also shows that the performance of the hybrid device than that of the CPV device is improved significantly.

In addition, it can be seen from Figs. 3–5 that in the region of $I > I_P$, both the power output and the efficiency of the hybrid device will decrease as the current I is increased for a given CG. Obviously, the region of $I > I_P$ is not the optimal operating region of the hybrid device. Thus, according to operating condition of the TEG, the optimal operating regions of the current I and the dimensionless current j for the CPV–TEG hybrid device should be determined by

$$I \le I_P \tag{22}$$

and

$$j_P \le j \le Z(T_H - T_L) \tag{23}$$

According to the optimum criterions of the current I, dimensionless current j and Figs. 3–5, one can further determine the optimum regions for the power output and operating temperature as

$$P_o \le P \le P_{max}, \tag{24}$$

and

$$T_{min} \le T \le T_{oper}, \tag{25}$$

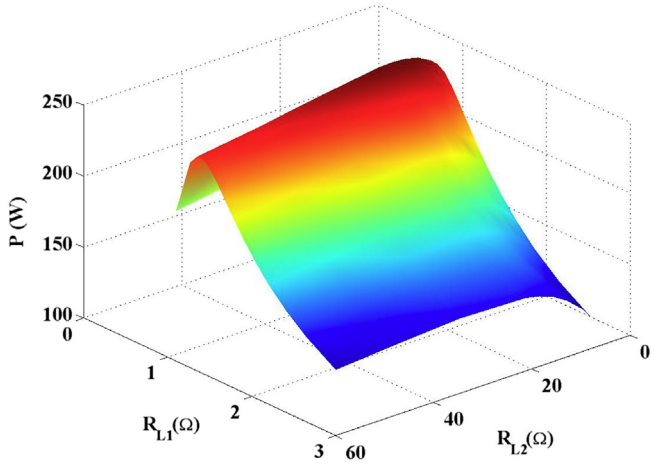

Fig. 6. The variation of the power output P with respect to R_{L1} and R_{L2} for some given parameters, where $G = 800$ W m^{-2}, $U_h A_h = 120$ W K^{-1} and $C = 5$ are chosen. The other given parameters are the same as those used in Fig. 3.

where P_o and T_{oper} are, respectively, the power output of the hybrid device and the operating temperature of the CPV module when the current of the CPV module is equal zero. It is clearly seen from Fig. 3 that in the optimally operating region, the power output and efficiency of the hybrid device are always larger than those the CPV module or TEG module. It shows once again that the application of the hybrid device may effectively improve the performance of the CPV system. This indicates that the hybrid system be more effective in the use of solar energy and improves the conversion efficiency of solar energy.

In order to understand further the general performance characteristics of the hybrid device, Eqs. (2)–(4), (18)–(20), and data in Tables 1 and 2 can be used to plot a three-dimensional graph (P, R_{L1}, R_{L2}), and the maximum power output P_{max}, corresponding optimal efficiency η_m and load matching versus CG curves, as shown in Figs. 6–8. It is seen from Fig. 6 that the power output of the hybrid device first increases and then decreases as R_{L1} and R_{L2} increase. It shows clearly that there are the optimal values of R_{L1} and R_{L2} at which the power output attains its maximum value for some given parameters. For example, when $CG = 4000$ W m^{-2} and data in Tables 1 and 2 are used, the maximum power output of the hybrid device occurs at $R_{L1opt} = 0.72$ Ω and $R_{L2opt} = 9.60$ Ω. For different choices of CG, R_{L1opt} and R_{L2opt} will have different optimal values and the maximum power output will also be different. It can be seen from Figs. 7 and 8 that the P_{max} and R_{L2opt} are monotonically

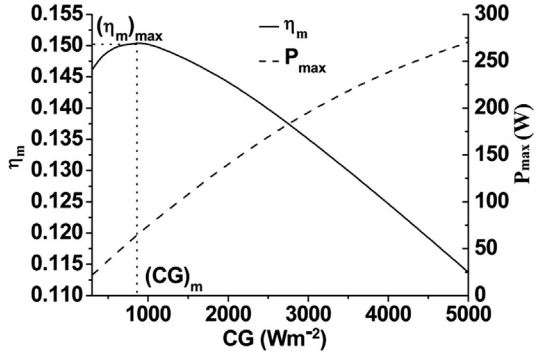

Fig. 7. The curves of the maximum power output P_{max} and corresponding optimal efficiency η_m varying with CG, where some given parameters are the same as those used in Fig. 3.

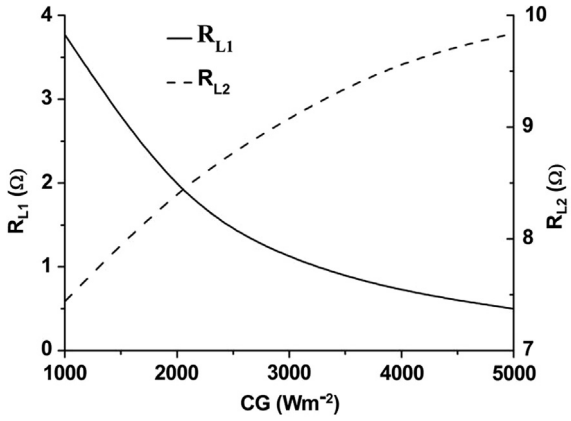

Fig. 8. The optimal load matching R_{L1opt} and R_{L2opt} varying with CG, where some given parameters are the same as those used in Fig. 3.

increasing function of G, while R_{L1opt} is a monotonically decreasing function of G. Fig. 7 shows that the efficiency at the maximum power output first increases and then decreases as CG is increased. It clearly shows that there exists an optimum value for CG at which η_m attains its maximum, i.e., $(\eta_m)_{max}$. It is seen the curves in Fig. 7 that when $\eta_m < (\eta_m)_{max}$, there are two corresponding CG for given some parameters, where one is smaller than $(CG)_m$ and the other is larger than $(CG)_m$. For a practical generator, one always hopes to obtain the power output as large as possible in the same efficiency. Thus, a photovoltaic–thermoelectric hybrid devices should be operated in the following region:

$$CG \geq (CG)_m \tag{26}$$

Obviously, Eq. (26) may provide an important criterion for distinguishing whether a CPV–TEG hybrid device is operated in the optimal states.

4. Conclusions

With the help of the model of a CPV–TEG hybrid system including multi-irreversibilities such as conduction and radiation heat losses in the concentrator, heat leak from the CPV to the environment, finite-rate heat transfer between the CPV and TEG, expressions for the power output and efficiency of the hybrid system are derived, from which the general performance characteristics of the hybrid system are revealed and the optimum criteria of some important parameters are determined. It can be found that the CPV–TEG hybrid generator system can provide not only more electric power but also higher efficiency than a CPV or TEG. The results obtained here may provide some theoretical basis for the optimal design and operation of practical CPV–TEG hybrid power generation system.

Acknowledgments

This work has been supported by the National Natural Science Foundation (No. 11175148), the Natural Science Foundation of Fujian Province (No. 2011J01012), and the Science Research Fund by Huaqiao University (No. 09BS510), People"s Republic of China.

References

[1] Yibing Gao, Hulin Huang, Yuehong Su, A parametric study of characteristics of concentrating PV modules, Int. J. Low-carbon Technol. 5 (2010) 57–62.

[2] Hamidreza Najafi, Keith A. Woodbury, Modeling and analysis of a combined photovoltaic-thermoelectric power generation system, J. Sol. Energy Eng 135 (2013), 031013-1–8.
[3] A. Royne, C.J. Dey, D.R. Mills, Cooling of photovoltaic cells under concentrated illumination: a critical review, Sol. Energy Mater. Sol. Cells 86 (2005) 451–483.
[4] S. Dubey, G.N. Tiwari, Thermal modeling of a combined system of photovoltaic thermal (PV/T) solar water heater, Sol. Energy 82 (2008) 602–612.
[5] A. Al-Alili, Y. Hwang, R. Radermacher, I. Kubo, A high efficiency solar air conditioner using concentrating photovoltaic/thermal collectors, Appl. Energy 93 (2012) 138–147.
[6] T.T. Chow, A review on photovoltaic/thermal hybrid solar technology, Appl. Energy 87 (2010) 365–379.
[7] Y. Vorobiev, J. González-Hernández, P. Vorobiev, L. Bulat, Thermal–photovoltaic solar hybrid system for efficient solar energy conversion, Sol. Energy 80 (2006) 170–176.
[8] F. Sarhaddi, S. Farahat, H. Ajam, A. Behzadmehr, Exergetic performance assessment of a solar photovoltaic thermal (PV/T) air collector, Energy Build 42 (2010) 2184–2199.
[9] S.A. Kalogirou, Y. Tripanagnostopoulos, Hybrid PV/T solar systems for domestic hot water and electricity production, Energy Convers. Manag. 47 (2006) 3368–3382.
[10] W.G.J.H.M. Van Sark, Feasibility of photovoltaic-thermoelectric hybrid modules, Appl. Energy 88 (2011) 2785–2790.
[11] Daniel Kraemer, Kenneth McEnaney, Matteo Chiesa, et al., Modeling and optimization of solar thermoelectric generators for terrestrial applications, Sol. Energy 86 (5) (2012) 1338–1350.
[12] Daniel Kraemer, Bed Poudel, Hsien-Ping Feng, et al., High-performance flat-panel solar thermoelectric generators with high thermal concentration, Nat. Mater. 10 (7) (2011) 532–538.
[13] T.M. Tritt, H. Böttner, L. Chen, Thermoelectrics: direct solar thermal energy conversion, MRS Bull. 33 (2008) 366–368.
[14] A. Muhtaroglu, A. Yokochi, A. Von Jouanne, Integration of thermoelectrics and photovoltaics as auxiliary power sources in mobile computing applications, J. Power Sources 177 (2008) 239–246.
[15] E.A. Chávez-Urbiola, Y.V. Vorobiev, L.P. Bulat, Solar hybrid systems with thermoelectric generators, Sol. Energy 86 (2012) 369–378.
[16] N.M.E. Khattab, T. El Shenawy, Optimal operation of thermoelectric cooler driven by solar thermoelectric generator, Energy Convers. Manag. 47 (2006) 407–426.
[17] D. Kraemer, L. Hu, A. Muto, X. Chen, G. Chen, M. Chiesa, photovoltaic–thermoelectric hybrid systems: a general optimization methodology, Appl. Phys. Lett. 92 (24) (2008) 243503.
[18] Nolwenn Le Pierres, Matthieu Cosnier, Lingai Luo, et al., Coupling of thermoelectric modules with a photovoltaic panel for air pre-heating and pre-cooling application; an annual simulation, Int. J. Energy Res. 32 (2008) 1316–1328.
[19] X. Zhang, K.T. Chau, An automotive thermoelectric-photovoltaic hybrid energy system using maximum power point tracking, Energy Convers. Manag. 52 (1) (2011) 641–647.
[20] X. Zhang, K.T. Chau, Design and implementation of a new thermoelectric–photovoltaic hybrid energy system for hybrid electric vehicles, Electric Power Compon. Syst. 39 (6) (2011) 511–525.
[21] N. Wang, L. Han, H. He, N.H. Park, K. Koumoto, A novel high-performance photovoltaic–thermoelectric hybrid device, Energy Environ. Sci. 4 (9) (2011) 3676–3679.
[22] Xing Ju, Zhifeng Wang, Gilles Flamant, et al., Numerical analysis and optimization of a spectrum splitting concentration photovoltaic–thermoelectric hybrid system, Sol. Energy 86 (6) (2012) 1941–1954.
[23] V. Leonov, T. Torfs, R.J.M. Vullers, C.V. Hoof, Hybrid thermoelectric–photovoltaic generators in wireless electroencephalography diadem and electrocardiography shirt, J. Electron. Mater. 39 (9) (2010) 1674–1680.
[24] G. Rockendorf, R. Sillmann, L. Podlowski, B. Litzenburger, PV-hybrid and thermoelectric collectors, Sol. Energy 67 (1999) 227–237.
[25] Daniel Kraemer, Bed Poudel, Hsien-Ping Feng, et al., High-performance flat-panel solar thermoelectric generators with high thermal concentration, Nat. Mater. 10 (7) (2011) 5325–5538.
[26] H.J. Goldsmid, J.E. Giutronich, M.M. Kaila, Solar thermoelectric generation using bismuth telluride alloys, Sol. Energy 24 (5) (1980) 435–440.
[27] G. Rockendorf, R. Sillmann, L. Podlowski, B. Litzenburger, PV-hybrid and thermoelectric collectors, Sol. Energy 67 (45–6) (1999) 227–237.
[28] G.J. Yu, Y.S. Jung, J.Y. Choi, et al., A novel two mode MPPT control algorithm based on comparative study of existing algorithms, Sol. Energy 76 (4) (2004) 454–463.
[29] Todd Otanicar, Ihtesham Chowdhury, Patrick E. Phelan, et al., Parametric analysis of a coupled photovoltaic/thermal concentrating solar collector for electricity generation, J. Appl. Phys. 108 (2010) 114907.
[30] Kashif Ishaque, Zainal Salam, Hamed Taheri, et al., Modeling and simulation of photovoltaic (PV) system during partial shading based on a two-diode model, Simul. Model. Pract. Theory 19 (2011) 1613–1626.
[31] J. Verschraegen, M. Burgelman, J. Penndorf, Temperature dependence of the diode ideality factor in CuInS 2-on-Cu-tape solar cells, Thin Solid Films 480–481 (2005) 307–311.
[32] Yuzhuo Pan, Bihong Lin, Jincan Chen, Performance analysis and parametric optimal design of an irreversible multi-couple thermoelectric refrigerator under various operating conditions, Appl. Energy 84 (9) (2007) 862–872.
[33] D.M. Rowe (Ed.), Thermoelectrics Handbook: Macro to Nano, CRC Press, London, NY, USA, 2006.
[34] D.M. Rowe (Ed.), CRC Handbook of Thermoelectrics, CRC Press, London, NY, USA, 1995.
[35] Gaowei Liang, Jiemin Zhou, Xuezhang Huang, Analytical model of parallel thermoelectric generator, Appl. Energy 88 (12) (2010) 1447–1454.
[36] S.B. Riffat, X. Ma, R. Wilson, Performance simulation and experimental testing of a novel thermoelectric heat pump system, Appl. Therm. Eng. 26 (2006) 494–501.
[37] R. Ahiska, K. Ahiska, New method for investigation of parameters of real thermoelectric modules, Energy Convers. Manag. 51 (2) (2010) 338–345.